Direct evidence for hidden one-dimensional Fermi surface of hexagonal $K_{0.25}WO_3$

S. Raj,[1,2,*] T. Sato,[1] S. Souma,[3] T. Takahashi,[1,3,4] D. D. Sarma,[5,6,†] Priya Mahadevan,[7] J. C. Campuzano,[8] M. Greenblatt,[9] and W. H. McCarroll[10]

[1]*Department of Physics, Tohoku University, Sendai 980-8578, Japan*
[2]*Department of Physics, Indian Institute of Science Education and Research, Kolkata 700 106, India*
[3]*WPI Advanced Institute for Materials Research, Tohoku University, Sendai 980-8577, Japan*
[4]*CREST, Japan Science and Technology Agency (JST), Kawaguchi 332-0012, Japan*
[5]*Centre for Advanced Materials, Indian Association for the Cultivation of Science, Kolkata 700 032, India*
[6]*Solid State and Structural Chemistry Unit, Indian Institute of Science, Bangalore 560 012, India*
[7]*S. N. Bose National Centre for Basic Sciences, JD Block, Sector 3, Salt Lake, Kolkata 700 098, India*
[8]*Department of Physics, University of Illinois at Chicago, Chicago, Illinois 60607, USA*
[9]*Department of Chemistry and Chemical Biology, The State University of New Jersey, Piscataway, New Jersey 08854, USA*
[10]*Department of Chemistry and Biochemistry, Rider University, Lawrenceville, New Jersey 08648, USA*

(Received 23 May 2008; published 18 June 2008)

The electronic structure of hexagonal potassium tungsten bronze $K_{0.25}WO_3$ has been investigated by high-resolution angle-resolved photoemission spectroscopy (ARPES). The experimentally determined band structure resolves the long-standing puzzles concerning the anomalous transport properties in this hexagonal bronze. We find that the ARPES-derived Fermi surface is the consequence of hidden one-dimensional (1D) bands, in good agreement with the calculated Fermi surface. These results indicate that the high-temperature anomaly in the electrical resistivity originates in the possible charge-density-wave formation associated with the hidden 1D Fermi surfaces.

DOI: 10.1103/PhysRevB.77.245120 PACS number(s): 71.18.+y, 71.30.+h, 79.60.−i

I. INTRODUCTION

The origin of unusual physical properties in transition-metal oxides has been a subject of intense research. Many low-dimensional compounds that one expects would be metallic exhibit anomalous transport properties that are often the result of a lattice instability leading to the formation of a charge-density wave (CDW). Various quasi-one-dimensional (1D) and quasi-two-dimensional (2D) molybdenum bronzes[1,2] show such instabilities and are well documented by the structural, spectroscopic, and transport measurements. This phenomenon has been intensively investigated with the close proximity of the CDW regime and the existence of superconductivity in several systems.[3–6] One class of materials that has received considerable attention is the hexagonal alkali-metal-doped tungsten bronzes. These systems have been found to exhibit superconductivity at low temperatures,[7–9] while exhibiting anomalies in the electrical resistivity suggestive of CDWs at high temperatures as seen in other systems.[10–13] Considering the example of K_xWO_3, one finds that the corner-shared WO_6 octahedra form six-membered rings, which form a channel [Fig. 1(a)]. The K atom sits at the center of one such channel. Resistivity measurements as well as Hall voltage and Seebeck coefficient measurements have established that the characteristic temperature T_B is a strong function of the alkali-metal concentration, exhibiting a maximum for $x=0.25$.[9] Several models, which include the formation of a CDW, an alkali-metal concentration-dependent crystallographic phase change,[14] and an ordering of the alkali-metal ions, have been proposed to explain this anomaly. These ambiguities still exist due to the lack of detailed information on the electronic structure of the system, especially about the states in the vicinity of the Fermi level (E_F). Hence a careful analysis of the band structure and Fermi surface (FS) investigation can establish the validity of various models as well as explain the origin of anomalous physical properties.

In this paper, we report results of high-resolution angle-resolved photoemission spectroscopy (ARPES) on $K_{0.25}WO_3$ and show that the FS consists of quasi-1D-like segments favorable to the formation of CDW, which would be respon-

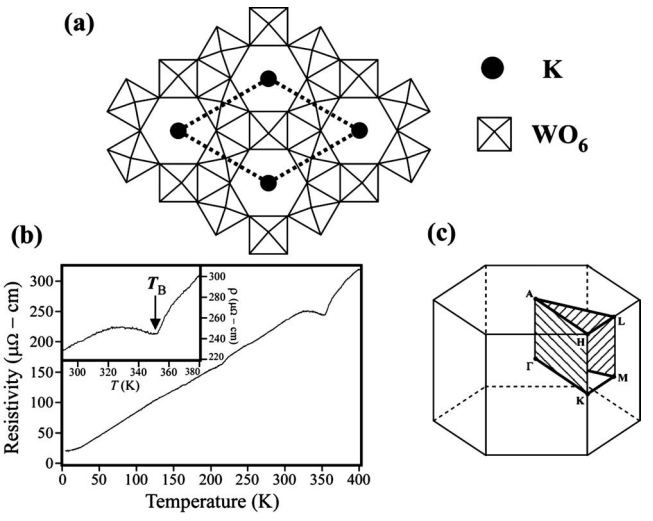

FIG. 1. (a) Crystal structure of K_xWO_3 projected onto the plane perpendicular to the c axis. Rhombus represents a unit cell. (b) Electrical resistivity of $K_{0.25}WO_3$ as a function of temperature. Inset shows the plot of expansion of resistivity around 350 K, and T_B is the temperature at which the resistivity shows a local minimum. (c) Brillouin zone of hexagonal K_xWO_3 showing high-symmetry lines.

sible for the characteristic transport anomaly at high temperatures. We demonstrate that both the experimentally obtained and the calculated FSs satisfy a nesting condition with commensurate wave vectors, in accordance with electron diffraction experiments.[15,16]

II. EXPERIMENTS

Hexagonal single crystals of $K_{0.25}WO_3$ were grown by fused salt electrolysis of K_2WO_4 and WO_3. The Laue diffraction pattern and the resistivity measurements show that the crystals are metallic with a single hexagonal phase. The resistivity measurement of $K_{0.25}WO_3$ is carried out by a conventional four-probe method and the result is shown in Fig. 1(b). $K_{0.25}WO_3$ shows metallic behavior for the full range of temperature along with a high-temperature anomaly around T_B=350 K, as shown in the inset of Fig. 1(b). ARPES measurements along the $\Gamma(A)$-$M(L)$ direction of the Brillouin zone (BZ) [Fig. 1(c)] were performed using a high-resolution spectrometer with a VG-SCIENTA R4000 electron analyzer with 22 eV photons at the undulator 4m-NIM beam line at the Synchrotron Radiation Center in Wisconsin. The energy and angular resolutions were set at 15 meV and 0.7°, respectively. We have used the wide-angle (38°) mode of the analyzer. A clean surface of the sample for ARPES measurements was obtained by *in situ* cleaving along the (001) surface.

III. BAND CALCULATIONS

We performed *ab initio* band-structure calculations for hexagonal WO_3 and compared them with the experimental band-structure calculations. A plane-wave basis was used with projected-augmented wave potentials[17,18] as implemented in the VASP code.[19] The generalized gradient approximation to the exchange functional was used, and the Kohn-Sham equations were solved over a k-point mesh involving $12\times12\times12$ points. The lattice constants were kept fixed at experimentally determined values of a=7.38 Å and c =7.513 Å. Internal parameters were allowed to relax. The effect of K doping was simulated within a rigid band model.

IV. RESULTS AND DISCUSSION

Figure 2(a) shows the valence-band ARPES spectra of $K_{0.25}WO_3$ measured at 20 K with 22 eV photons along the $\Gamma(A)$-$M(L)$ direction. WO_3 has a large band gap of 2 eV, and due to the K doping the Fermi energy moves about 1 eV into the conduction band of WO_3. As a result the valence band of WO_3 starts at energies of ~3 eV below the Fermi energy. There are three prominent peaks visible along the $\Gamma(A)$-$M(L)$ direction. The nondispersive edge of the valence band (at 3.0 eV) is prominent around $\Gamma(A)$ point and loses its intensity around the zone boundary. The most prominent dispersive peaks in the valence band are seen at 4.5 and 6.0 eV at $\Gamma(A)$. To see dispersive bands clearly, we plot in Fig. 2(b) the second derivative of the ARPES spectral intensity by gradual shading as a function of the wave vector and the binding energy. The bright areas correspond to the experimental bands. We also show the pseudopotential band structure of

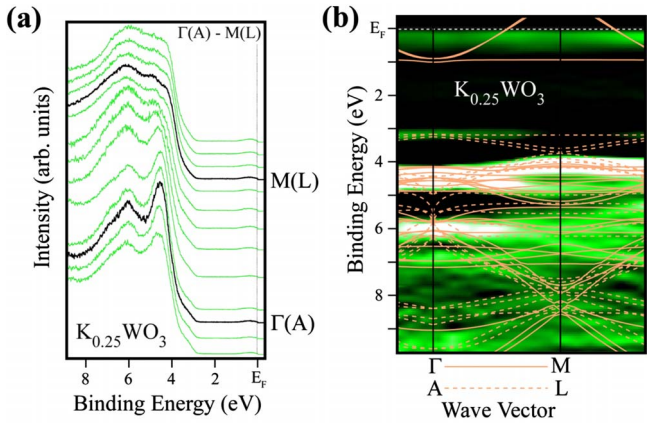

FIG. 2. (Color online) (a) Valence-band ARPES spectra of $K_{0.25}WO_3$ measured along $\Gamma(A)$-$M(L)$ cut at 20 K with 22 eV photon energy. (b) Experimentally determined valence-band structure along $\Gamma(A)$-$M(L)$ direction obtained from the ARPES experiments. The white bright areas correspond to the experimental bands. Theoretical band structure of hexagonal WO_3 after shifting position of E_F is also shown by the thin, solid, and dashed lines.

hexagonal WO_3 for comparison. The calculated Fermi energy has been shifted to account for the band-gap underestimation that is usually found in first-principles calculations. The top of the valence band at 3.0 eV around $\Gamma(A)$ originates in the *AHL* plane and is well explained by the band calculation. The dispersion of other bands along the $\Gamma(A)$-$M(L)$ direction is in good agreement with the band calculation. From the *ab initio* calculations, we conclude that the valence band (3–9 eV) has predominantly O $2p$ character with a small admixture of bonding W $5d$ e_g character.

The anomalous physical properties are governed by the electronic states in the vicinity of E_F; therefore we have carried out high-resolution ARPES measurements of conduction band near E_F with a smaller energy interval and a higher signal-to-noise ratio. Figure 3(a) shows the ARPES spectra near E_F of $K_{0.25}WO_3$ measured at 20 K with 22 eV photons along the $\Gamma(A)$-$M(L)$-$\Gamma(A)$ direction. The spectral intensity of energy distribution curves (EDCs) is normalized by the integrated intensity at 1.0–1.5 eV binding energy. As seen in Fig. 3(a), it is hard to observe dispersive features near E_F from EDCs, while finite intensity modulation is observed around 0.4 eV. This weakly dispersive nature of bands is most likely due to the high background from angle-integrated spectra and disorder effect as observed in the analogous series, Na_xWO_3, where alkali-ion disorder creates a large Coulomb gap near E_F.[20,21] In Fig. 3(b), we plot the ARPES intensity as a function of the wave vector and the binding energy. We have superimposed calculated bands that cross the Fermi energy according to the *ab initio* band-structure calculation and have found that the intensity modulations show a close correlation with the positions of calculated bands. The periodicity between the calculated bands and the intensity modulation of the ARPES spectra is quite similar even in the second BZ. The character of these bands crossing the Fermi energy is found to be derived from primarily xz/yz orbitals. Hence in $K_{0.25}WO_3$, the π band resulting from the xz/yz orbitals is responsible for the observed

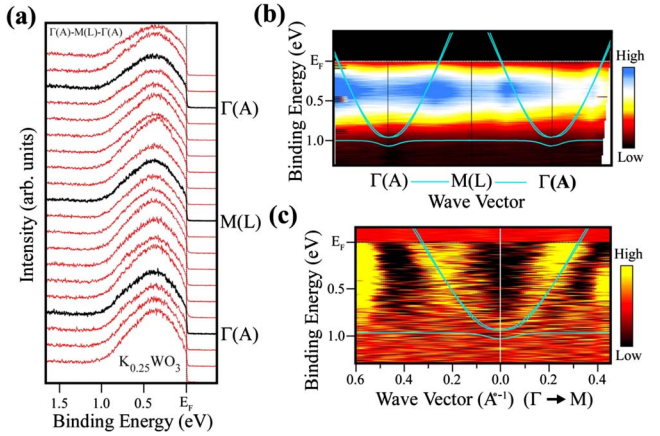

FIG. 3. (Color online) (a) ARPES spectra near E_F of $K_{0.25}WO_3$ measured along $\Gamma(A)$-$M(L)$-$\Gamma(A)$ cut at 20 K with 22 eV photon energy. (b) ARPES-intensity plot near E_F as a function of wave vector and binding energy measured along $\Gamma(A)$-$M(L)$-$\Gamma(A)$ cut, together with the calculated bands (solid lines). (c) Plot of the second derivative of MDC and the calculated bands (solid lines) around $\Gamma(A)$ point along the $\Gamma(A)$-$M(L)$ direction.

transport properties. In Fig. 3(c), the second derivative of momentum distribution curves (MDCs) is shown in the $(E\text{-}k)$ space to visualize the band dispersions. Since the bands disperse very fast, it is expected that the dispersion will be more clearly visible in the second derivative of MDC analysis, which has been successfully applied to other systems.[22] As seen in Fig. 3(c), the experimental band dispersion matches well with the band calculation, and the bottom of conduction band extends up to 1 eV binding energy.

In Fig. 4(a), we show ARPES-intensity plot at E_F as a function of a two-dimensional wave vector. The intensity is obtained by integrating the spectral weight within ± 10 meV with respect to E_F. As clearly seen in Fig. 4, the FS appears to show almost straight behavior along alternating K-K directions (i.e., along $\Gamma(M)$ direction) in metallic $K_{0.25}WO_3$, indicating the presence of nearly 1D FS. We also calculated the FS for $K_{0.25}WO_3$ by assuming a rigid shift of E_F in hexagonal WO_3 and compared it with the experimental FS as solid line in Fig. 4(a). There is no band crossing at E_F in AHL plane, and the FS is only from bands in the ΓKM plane. In the calculation, FS consists of two trianglelike electron pockets centered at Γ point and six small hole pockets at the K points. The calculated FSs on the ΓKM plane essentially trace the experimentally observed FS in their location and topology. The straight segment in the calculation that connects one K point to another K point is clearly observed in the ARPES experiments, demonstrating that the FS of $K_{0.25}WO_3$ is essentially explained by the hidden 1D-like character of the bands. We think that the high-temperature anomaly in the resistivity of $K_{0.25}WO_3$ is due to the CDW transition and may be explained by the well-nested character of bands and/or FSs. The CDW might be a weaker and/or fluctuating one in $K_{0.25}WO_3$ since the resistivity jump at T_B is not significant as compared to other well-known CDW materials (sometimes it jumps one or two orders in resistivity across the transition temperature). Also, weak and/or fluctuating CDW materials usually satisfy other conditions such as

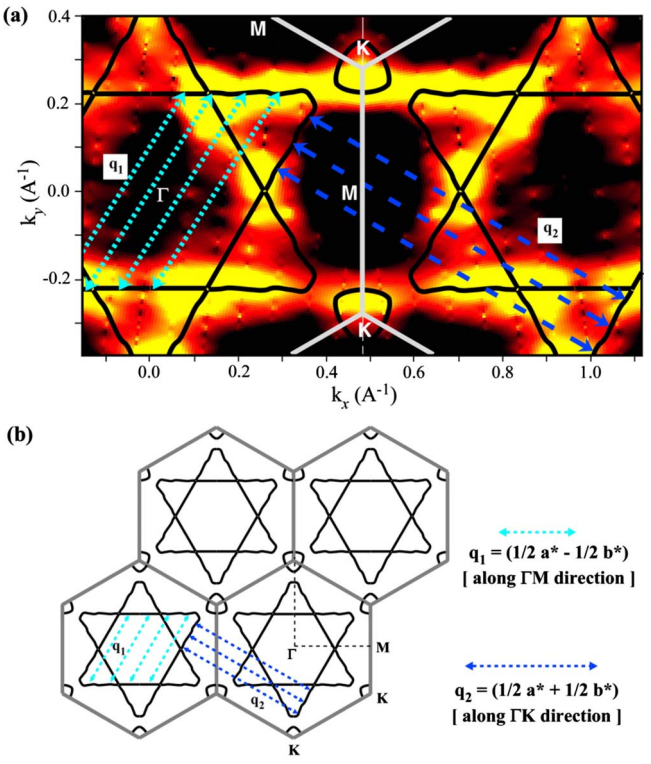

FIG. 4. (Color online) (a) ARPES spectral intensity of $K_{0.25}WO_3$ within ± 10 meV with respect to E_F plotted as a function of two-dimensional wave vector. The FS topology is extended to second BZ by symmetrizing the experimental plot. The bright areas correspond to the experimentally obtained FS. The thick solid lines are the calculated FSs on the ΓKM plane for $K_{0.25}WO_3$. The nesting vectors q_1 and q_2 along the ΓM and ΓK directions, respectively, are also shown by the thick dashed arrows. (b) Calculated FSs and possible superlattice vectors $q_1=(\frac{1}{2}a^*-\frac{1}{2}b^*)$ and $q_2=(\frac{1}{2}a^*+\frac{1}{2}b^*)$ along the ΓM and ΓK directions, respectively.

the well- (or partially) nested FS and the superlattice reflections in diffraction measurements below T_B. Our ARPES measurements reveal the existence of straight 1D FSs, which can be well nested by the nesting vectors q_1 and q_2. Similar phenomena have also been observed in other CDW systems such as $NbSe_3$ and $ZrTe_3$,[11,23–26] which show metallic behavior even below the CDW-transition temperature (T_{CDW}). Since the FSs of W $5d$ t_{2g} orbital are nested, it is hard to attribute the origin of characteristic transport anomaly to the simple alkali-ion-dependent crystallographic structural change or the ordering of K ions because the FS nesting of W $5d$ band is less related to these phenomena. In $K_{0.25}WO_3$, K donates its $4s$ electron to W $5d$ t_{2g} band, and it finds that the conduction band is mainly from W $5d$ t_{2g} band, which is responsible for all the physical properties of $K_{0.25}WO_3$. Our finding reveals that these W $5d$ t_{2g} bands form 1D-like FSs. Few strongly correlated transition metal oxide systems also show similar 1D-like FSs due to electronic phase separation; i.e., a high concentration of mobile carriers are separated from those of low concentration due to Coulomb interactions, which is known as "stripes." In hole-doped high-Tc cuprate superconductors,[27–30] stripes are due to the intrinsically inhomogeneous distribution of spin and charge in the

CuO_2 sheets. Similarly in hole-doped nickelates,[31–34] stripes are associated with the NiO_2 sheets. These charge stripes reflect a 1D topology and are generally associated with the mobile carriers responsible for the FS of the system. In our $K_{0.25}WO_3$ system, FS comes from the W $5d$ character so that the K ion ordering is less related to the observed phenomena.

Now we discuss FS nesting quantitatively in relation to the diffraction experiments. The periodic lattice distortion leading to the formation of CDW always gives rise to superlattice reflections at the nesting vector q in diffraction measurements. Indeed, electron[15] and powder neutron diffraction[16] studies observed superlattice reflections below T_B. Electron diffraction studies have revealed two types of superlattice reflections: (i) closely spaced incommensurate reflections along rows perpendicular to the a^*-b^* plane (c^* direction) and (ii) commensurate superlattice reflections within the a^*-b^* plane. From the various diffraction data it was found that the superlattice vectors are $\frac{1}{2}a^*$ and $\frac{1}{2}b^*$, and the incommensurate reflections along the c^* direction may be originating from each of the regular $hk0$ reflections or from the commensurate superlattice reflections. The commensurate superlattice reflections in $K_{0.25}WO_3$ indicate a different orthohexagonal symmetry of the superlattice and the resulting superlattice vectors are $(\frac{1}{2}a^*-\frac{1}{2}b^*)$ and $(\frac{1}{2}a^*+\frac{1}{2}b^*)$. These incommensurate superlattice reflections along the c^* direction and commensurate superlattice reflections in the a^*-b^* plane in $K_{0.25}WO_3$ imply that the superlattice vectors essentially have two different characters. In the present ARPES experiment, we found that the directions of superlattice vectors $(\frac{1}{2}a^*-\frac{1}{2}b^*)$ and $(\frac{1}{2}a^*+\frac{1}{2}b^*)$ are along the $\Gamma(M)$ and $\Gamma(K)$ directions, respectively. The amplitude of superlattice vector $(\frac{1}{2}a^*-\frac{1}{2}b^*)$ matches quantitatively well with the nesting vector q_1 derived from our FS mapping along the $\Gamma(M)$ direction. The calculated FS also shows three 1D-like bands around Γ in the ΓKM plane, which is in excellent agreement with the experimental FS. We also observed evidence of a piece of the FS near the K points in accordance with the calculated hole pockets. However, the hybridization gap is not clearly observed in the experimental FS. In Fig. 4(b), we show the possible nesting vectors along the $\Gamma(M)$ and $\Gamma(K)$ directions. We found that straight FS segments are well connected by two vectors, namely, $(\frac{1}{2}a^*-\frac{1}{2}b^*)$ and $(\frac{1}{2}a^*+\frac{1}{2}b^*)$. The nesting vector $(\frac{1}{2}a^*+\frac{1}{2}b^*)$ along the $\Gamma(K)$ direction connects the FS of the first BZ to the second BZ.

The existence of finite Fermi edge in Fig. 3(a) suggests that the FS of $K_{0.25}WO_3$ is not nested in all momentum regions and the ungapped momentum region would still remain below T_B. We do not know the exact location of the ungapped momentum region, possibly because of the momentum broadening due to strong scattering. The residual FS should be responsible for the metallic transport properties below T_B. It is noted here that in K_xWO_3, superconductivity completely vanishes for $x=0.25$ in contrast to the enhancement of T_B value (possibly CDW transition temperature). We think that the remaining FS segments do not contribute to the superconductivity at $x=0.25$ because CDW fluctuation associated with the hidden 1D-like FS sheets would be strongest and would completely suppress the superconducting coherence by the scattering of electrons among the nested and metallic FSs. We also believe that when the doping changes, FSs are not able to keep good nesting conditions, which would be favorable to the recovery of superconductivity away from $x=0.25$.

V. CONCLUSION

We have directly determined the band dispersion and Fermi surface of hexagonal potassium tungsten bronze $K_{0.25}WO_3$ by high-resolution ARPES. The experimentally determined electronic band structure resolves the long-standing puzzles of anomalous transport properties. We found that the Fermi surface is the consequence of hidden one-dimensional-like bands. The nesting vector q_1 derived from the ARPES experiments matched very well with the commensurate superlattice reflection vector $(\frac{1}{2}a^*-\frac{1}{2}b^*)$ obtained from the electron diffraction experiments. We conclude that the possible CDW formation due to the presence of hidden 1D-like bands and/or FSs is responsible for the anomalous transport properties.

ACKNOWLEDGMENTS

This work is supported by grants from JSPS, CREST-JST, and MEXT of Japan. The Synchrotron Radiation Center is supported by NSF-DMR under Grant No. 0084402. S.R. acknowledges the financial support from JSPS. The work within India was supported by DST, India. The work at Rutgers was supported by NSF-DMR Grants No. 0541911 and No. 0233697.

*raj@arpes.phys.tohoku.ac.jp

†Also at Jawaharlal Nehru Centre for Advanced Scientific Research, Bangalore 560 054, India.

[1] L. Perfetti, S. Mitrovic, G. Margaritondo, M. Grioni, L. Forro, L. Degiorgi, and H. Hochst, Phys. Rev. B **66**, 075107 (2002).

[2] C. Schlenker, *Low Dimensional Electronic Properties of Molybdenum Bronzes and Oxides* (Kluwer, Dordrecht, 1989).

[3] S. Nagata, T. Aochi, T. Abe, S. Ebisu, T. Hagino, Y. Seki, and K. Tsutsumi, J. Phys. Chem. Solids **53**, 1259 (1992).

[4] T. Kumakura, H. Tan, T. Handa, M. Morishita, and H. Fukuyama, Czech. J. Phys. **46**, 2611 (1996).

[5] D. Jaiswal, A. A. Tulapurkar, S. Ramakrishnan, A. K. Grover, G. J. Nieuwenhuys, and J. A. Mydosh, Physica B **312–313**, 142 (2002).

[6] Y. Singh, R. Nirmala, S. Ramakrishnan, and S. K. Malik, Phys. Rev. B **72**, 045106 (2005).

[7] R. K. Stanley, R. C. Morris, and W. G. Moulton, Solid State Commun. **27**, 1277 (1978); Phys. Rev. B **20**, 1903 (1979).

[8] M. R. Skokan, W. G. Moulton, and R. C. Morris, Phys. Rev. B **20**, 3670 (1979).
[9] L. H. Cadwell, R. C. Morris, and W. G. Moulton, Phys. Rev. B **23**, 2219 (1981).
[10] P. Monceau, N. P. Ong, A. M. Portis, A. Meerschaut, and J. Rouxel, Phys. Rev. Lett. **37**, 602 (1976).
[11] N. P. Ong and P. Monceau, Phys. Rev. B **16**, 3443 (1977).
[12] R. M. Fleming, D. E. Moncton, and D. B. McWhan, Phys. Rev. B **18**, 5560 (1978).
[13] E. Canadell and M. H. Whangbo, Inorg. Chem. **29**, 1398 (1990).
[14] The normal electrical transport properties of for $x \leq 0.33$ show anomalous behavior in high temperature while those of Cs_xWO_3 do not.
[15] H. B. Krause, W. G. Moulton, and R. C. Morris, Acta Crystallogr., Sect. B: Struct. Sci. **41**, 11 (1985).
[16] J. Schultz, H. Horiuchi, and H. B. Krause, Acta Crystallogr., Sect. C: Cryst. Struct. Commun. **42**, 641 (1986).
[17] P. E. Blochl, Phys. Rev. B **50**, 17953 (1994).
[18] G. Kresse and D. Joubert, Phys. Rev. B **59**, 1758 (1999).
[19] G. Kresse and J. Furthmüller, Phys. Rev. B **54**, 11169 (1996); Comput. Mater. Sci. **6**, 15 (1996).
[20] S. Raj, D. Hashimoto, H. Matsui, S. Souma, T. Sato, T. Takahashi, S. Ray, A. Chakraborty, D. D. Sarma, P. Mahadevan, W. H. McCarroll, and M. Greenblatt, Phys. Rev. B **72**, 125125 (2005).
[21] S. Raj, D. Hashimoto, H. Matsui, S. Souma, T. Sato, T. Takahashi, D. D. Sarma, P. Mahadevan, and S. Oishi, Phys. Rev. Lett. **96**, 147603 (2006).
[22] T. Yoshida, K. Tanaka, H. Yagi, A. Ino, H. Eisaki, A. Fujimori, and Z. X. Shen, Phys. Rev. Lett. **95**, 146404 (2005).
[23] R. Yomo, K. Yamaya, M. Abliz, M. Hedo, and Y. Uwatoko, Phys. Rev. B **71**, 132508 (2005).
[24] J. Schäfer, E. Rotenberg, S. D. Kevan, P. Blaha, R. Claessen, and R. E. Thorne, Phys. Rev. Lett. **87**, 196403 (2001).
[25] J. Schäfer, M. Sing, R. Claessen, E. Rotenberg, X. J. Zhou, R. E. Thorne, and S. D. Kevan, Phys. Rev. Lett. **91**, 066401 (2003).
[26] T. Yokoya, T. Kiss, A. Chainani, S. Shin, and K. Yamaya, Phys. Rev. B **71**, 140504(R) (2005).
[27] J. M. Tranquada, B. J. Sternlieb, J. D. Axe, Y. Nakamura, and S. Uchida, Nature (London) **375**, 561 (1995).
[28] Y. Ando, K. Segawa, S. Komiya, and A. N. Lavrov, Phys. Rev. Lett. **88**, 137005 (2002).
[29] D. Reznik, L. Pintschovius, M. Ito, S. Iikubo, M. Sato, H. Goka, M. Fujita, K. Yamada, G. D. Gu, and J. M. Tranquada, Nature (London) **440**, 1170 (2006).
[30] T. Hanaguri, C. Lupien, Y. Kohsaka, D.-H. Lee, M. Azuma, M. Takano, H. Takagi, and J. C. Davis, Nature (London) **430**, 1001 (2004).
[31] V. Sachan, D. J. Buttrey, J. M. Tranquada, J. E. Lorenzo, and G. Shirane, Phys. Rev. B **51**, 12742 (1995).
[32] J. M. Tranquada, K. Nakajima, M. Braden, L. Pintschovius, and R. J. McQueeney, Phys. Rev. Lett. **88**, 075505 (2002).
[33] J. M. Tranquada, D. J. Buttrey, V. Sachan, and J. E. Lorenzo, Phys. Rev. Lett. **73**, 1003 (1994).
[34] J. M. Tranquada, J. E. Lorenzo, D. J. Buttrey, and V. Sachan, Phys. Rev. B **52**, 3581 (1995).